# Femtosecond Dynamics of the Methane−Methanol and Benzene−Phenol Conversions by an Iron−Oxo Species

**Kazunari Yoshizawa,* Yoshihito Shiota, Yoshihisa Kagawa, and Tokio Yamabe**

*Department of Molecular Engineering, Kyoto University, Sakyo-ku, Kyoto 606-8501, Japan, and Institute for Fundamental Chemistry, 34-4 Takano-Nishihiraki-cho, Sakyo-ku, Kyoto 606-8103, Japan*

*Received: July 20, 1999; In Final Form: January 11, 2000*

Femtosecond dynamic behavior of the methane−methanol conversion by the bare iron−oxo complex ($FeO^+$) is presented using the B3LYP density-functional-theory (DFT) method. We propose that the reaction pathway for the direct methane−methanol conversion is partitioned into the H atom abstraction via a four-centered transition state and the methyl migration via a three-centered transition state. It is demonstrated that both the H atom abstraction and the methyl migration occur in a concerted manner in a time scale of 100 fs. The concerted H atom abstraction and the direct H atom abstraction via a transition state with a linear C−H−O(Fe) array are compared. The direct H atom abstraction of methane is predicted to occur in a time scale of 50 fs. Isotope effects on the concerted and the direct H(D) atom abstractions are also computed and analyzed in the $FeO^+$/methane system. Predicted values of the kinetic isotope effect ($k_H/k_D$) for the H(D) atom abstraction of methane are 9 in the concerted mechanism and 16 in the direct abstraction mechanism at 300 K. Dynamics calculations are also carried out on the benzene−phenol conversion by the $FeO^+$ complex. The general profile of the electronic process of the benzene−phenol conversion is identical to that of the methane−methanol conversion with respect to essential bonding characters. It is demonstrated that the concerted H atom abstraction and the phenyl migration require 200 and 100 fs to be completed, respectively, in the $FeO^+$/benzene system.

## Introduction

The activation of the C−H bond of hydrocarbons, especially of methane,[1−9] has attracted increased attention in recent years because of its scientific and technological importance. The direct conversion of methane to methanol will be an important chemical process in the coming 21st century because the direct process is energetically efficient and would reduce the number of steps required, thus saving on capital costs in a commercial plant. Schröder and Schwarz[10,11] demonstrated that the bare $FeO^+$ complex, generated from $Fe^+$ and $N_2O$ under ion cyclotron resonance conditions, reacts with methane in the gas phase to produce methanol in 41% yield. The insertion intermediate, $HO-Fe^+-CH_3$, has been proposed to play a central role in this interesting gas-phase reaction.

We have proposed from density-functional-theory (DFT) computations that the methane−methanol conversion should proceed as shown in Scheme 1 via the two transition states (TS1 and TS2).[12] From detailed intrinsic reaction coordinate (IRC) analyses,[13] TS1 and TS2 were confirmed to correctly connect the reaction pathway for the conversion of methane to methanol. The reaction efficiencies and the methanol branching ratios[11] in the reactions of methane with $MnO^+$, $FeO^+$, and $CoO^+$ are nicely explained on the basis of the two-step concerted mechanism.[12b] This mechanism is in remarkable contrast to the so-called oxygen rebound mechanism,[14,15] in which a direct H atom abstraction via a transition state with a C−H−O(Fe) array is assumed to occur in the initial stages of the mechanism. We have applied this concerted mechanism to the methane hydroxylation by soluble methane monooxygenase (sMMO),[16] proposing that the conversion of methane to methanol should

**SCHEME 1**

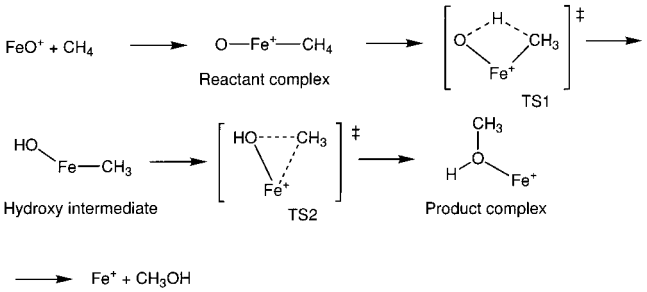


take place in a similar fashion in a diiron model complex[17] that involves an $Fe_2(\mu\text{-}O)_2$ diamond core, a possible model of intermediate **Q** of sMMO.[18] However, several possible mechanisms have been suggested for the methane hydroxylation by sMMO from theoretical and experimental viewpoints.[19] It has been proposed from DFT-computational analyses using dinuclear models[20] that the direct H atom abstraction should take place in the initial stages of hydrocarbon hydroxylations by sMMO.

Economical, direct conversion of benzene to phenol[21] has also attracted the attention of researchers in pure and applied chemistry for many years. Such a direct process for the hydroxylation of benzene was discovered in 1982 by Iwamoto et al.[22] as a gas-phase process over various transition-metal oxides supported on silica gel using nitrous oxide ($N_2O$) as an oxidizing reagent. ZSM-5 zeolite proved to show a higher catalytic selectivity for the oxidation of benzene to phenol. A surface oxygen species generated on Fe−ZSM-5 zeolite under $N_2O$-decomposition conditions has been proposed by Panov et al.[23] to be responsible for the high reactivity of the catalyst. From a different point of view, a similar direct benzene

* To whom all correspondence should be addressed at Kyoto University. E-mail: kazunari@scl.kyoto-u.ac.jp.

10.1021/jp992464t CCC: $19.00 
Published on Web 02/25/2000

**SCHEME 2**

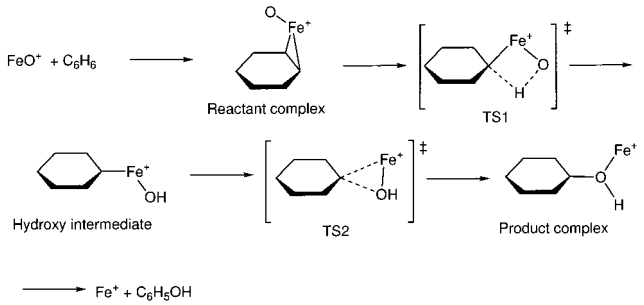


**SCHEME 3**

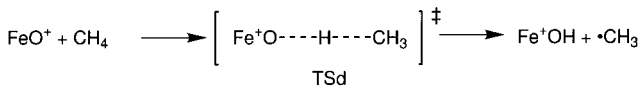


hydroxylation in the gas phase has been investigated by Schröder, Schwarz, and their collaborators.[24] The bare $FeO^+$ complex reacts with benzene under ion cyclotron resonance conditions, leading to the formation of $Fe^+/C_6H_5OH$ in 56% yield. They discussed possible reaction intermediates involving initial $FeO^+(C_6H_6)$ complexes of different structures.

We recently proposed that the direct conversion of benzene to phenol should occur also in the two-step manner with the hydroxy intermediate, as indicated in Scheme 2.[25] The reaction intermediates and the transition states in this reaction pathway are quite similar to those in the methane−methanol conversion pathway with respect to essential bonding characters. The mechanism for the gas-phase reactions may have relevance to some catalytic and enzymatic processes concerning hydrocarbon hydroxylations if coordinatively unsaturated transition-metal oxides are responsible for such important chemical reactions.

The kinetic isotope effect ($k_H/k_D$) is an important measure in discussing how H atom abstraction of a hydrocarbon substrate takes place in catalysts and enzymes. The oxygen rebound mechanism,[14,15] a widely believed radical mechanism, is supported by observed large kinetic isotope effects and considerable loss of stereochemistry at a carbon atom of the substrate. The initial step of this radical mechanism is indicated in Scheme 3. However, on the basis of the measured short "radical" lifetimes of 70−100 fs and regiochemical variations in enzymatic hydroxylations by cytochrome P450 and sMMO, Newcomb and collaborators[26] recently suggested in both P450- and sMMO-catalyzed hydroxylations a possible transition state of oxene insertion, which is essentially identical to the oxenoid model of Hamilton.[27] It is therefore of current interest to theoretically investigate the real time required for the abstraction of an H atom of the hydrocarbon substrate and its deuterium effects.

Filatov and Shaik[28] computed and analyzed three possible mechanisms, the oxygen rebound mechanism,[14,15] the two-step concerted mechanism,[19d] and the oxene-insertion mechanism,[27] in the reaction between $FeO^+$ and $H_2$, which leads to the formation of $Fe^+$ and $H_2O$, and concluded that the first and the second mechanisms are likely and competitive in energy in the H−H bond dissociation. However, the oxene insertion in the $FeO^+/H_2$ system was characterized by a high energy barrier, and its "transition state" was computed to have two imaginary modes of vibration, implying that it is not a true transition state. In line with their statement, we have not yet succeeded in obtaining a transition state for the oxene insertion into the C−H bond of methane like in Scheme 4 and we now think that the oxene insertion should be an unrealistic mechanism. In this study, we therefore confine our discussions on the oxygen rebound mechanism and the two-step concerted mechanism in the reactions of $FeO^+$ with methane and benzene.

**SCHEME 4**

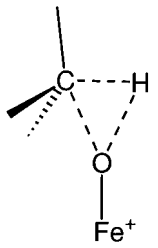


To the best of our knowledge, dynamics analysis has not yet been carried out for the C−H bond activation of alkanes and arenes catalyzed by transition-metal complexes. We therefore decided to run molecular dynamics simulations on potential energy surfaces at the B3LYP level of density functional theory.[29,30] We present some dynamic aspects of the methane−methanol and the benzene−phenol conversions by the bare iron−oxo complex. The behavior of the reaction intermediates and the undetectable transition states along the interesting reaction pathways indicated in Schemes 1 and 2 and its isotope effects are specifically discussed. The direct H atom abstraction of methane by the $FeO^+$ complex is also computed and analyzed. From the real-time dynamics analysis one can obtain useful information concerning the reaction pathways for the transition-metal catalyzed hydroxylations of methane and benzene.

## Method of Calculation

We used the B3LYP method, a hybrid Hartree−Fock/density-functional-theory (DFT) method in this work. This hybrid method consists of the Slater exchange, the Hartree−Fock exchange, the exchange functional of Becke,[29] the correlation functional of Lee, Yang, and Parr (LYP),[30] and the correlation functional of Vosko, Wilk, and Nusair[31] and has been successfully applied to many reactions catalyzed by transition-metal complexes. We can evaluate the applicability of this method from the dissociation energy of the $^6\Sigma^+$ state of $FeO^+$; the B3LYP method behaves better than the QCISD(T) and the CASPT2 methods for this quantity to give a value consistent with an experiment, as indicated previously.[25] Thus, the method of choice is appropriate for the subject of this paper. For the Fe atom we used the (14s9p5d) primitive set of Wachters[32] supplemented with one polarization f function ($\alpha = 1.05$)[33] resulting in a (611111111|51111|311|1) [9s5p3d1f] contraction. For the H, C, and O atoms, we used the 6-311G** basis set[34] in the $FeO^+/CH_4$ system and the D95** basis set[35] in the $FeO^+/C_6H_6$ system. Transition states were optimized and characterized from vibrational analyses; they were confirmed to have only one imaginary mode of vibration. The Gaussian 94 program[36] was used for the DFT computations.

Newton's equations of motion were solved to determine positions, velocities, and accelerations for each atom. We used for the dynamics calculations a standard velocity Verlet algorithm:[37]

$$r_i^{n+1} = r_i^n + v_i^n \Delta t + \frac{\Delta t^2}{2m_i} f_i^n \quad (1)$$

$$v_i^{n+1} = v_i^n + \frac{\Delta t}{2m_i}(f_i^{n+1} + f_i^n) \quad (2)$$

in which $r_i$ is the site of atom $i$ with mass $m_i$, $v_i$ is the velocity,

$f_i$ is the force, and $n$ is the step number. We took a time interval $\Delta t$ of 0.5 fs, which is short enough compared to 12 fs for the period of C−H stretching vibration. The forces were calculated with the B3LYP DFT method according to eq 3, where $E^n$ is

$$f_i^n = -\nabla E^n \tag{3}$$

the potential energy of a reacting system in the $n$th step. The femtosecond dynamics calculations were carried out by solving the equations of motion with a program written in our group. To start the dynamics calculation, small kinetic energy was supplied to a transition state toward both reactant and product directions along the imaginary mode of vibration while the total energy is conserved throughout the reaction. Thus, the reacting system has excess kinetic energy in both the reactant and the product whereas it has almost no kinetic energy in the vicinity of the transition state. The trajectory obtained within the framework of this methodology is close to the corresponding IRC. Since the reacting system passes over the transition state with infinitesimal velocity, the energy profile of the obtained dynamic reaction coordinate is flat near the transition state, as we see later in this paper. We therefore think that this procedure would provide an upper limit of the minimum possible time required for a chemical reaction. If the system has much kinetic energy in the transition state, the reaction would be significantly accelerated along the IRC.

## Methane−Methanol Conversion

**Reaction Pathway for the Two-Step Concerted Mechanism.** The reaction pathway for the direct methane−methanol conversion is partitioned into the H atom abstraction via the four-centered TS1 and the methyl migration via the three-centered TS2, as indicated in Scheme 1. Detailed descriptions of the reaction intermediates and the transition states as well as of the energetics can be seen in our previous papers.[12] The first issue that we address in this paper is the femtosecond dynamics of the H atom abstraction, in which the C−H bond dissociation and the O−H bond formation take place in a concerted manner. Figure 1 presents a computed potential energy profile for the H atom abstraction of methane in the $FeO^+/CH_4$ system via the TS1 along the dynamic reaction coordinate of the sextet state. The indicated relative energy is measured from the dissociation limit of the reactants of the ground state, i.e., $CH_4$ and the bare $FeO^+$ complex of the sextet state ($^6\Sigma^+$). Snapshots of the structures of the system along the dynamic reaction coordinate are also indicated in the illustration. The TS1 of the sextet state was computed at the C−H bond distance of 1.43 Å and at the O−H bond distance of 1.30 Å. The activation barrier for this step amounts to 31.1 kcal/mol when measured from the reactant complex. This reaction starts with the formation of the reactant (methane) complex and ends with the formation of the hydroxy intermediate ($HO-Fe^+-CH_3$). In the actual procedure of calculation, we supplied kinetic energy of 0.1 kcal/mol to the transition state toward both reactant and product directions in order to start the dynamic calculations. Here we defined the transition state as 0 fs in the time scale. Since this method conserves the total energy of the system, the sum of potential and kinetic energy is constant and the change in potential energy is distributed to intramolecular movements as kinetic energy.

Let us look in detail at the dynamic reaction coordinate of the reaction in the $FeO^+/CH_4$ system. The methane molecule and the bare $FeO^+$ complex come into contact to lead to the $OFe^+(CH_4)$ complex in the initial stages of the reaction. This

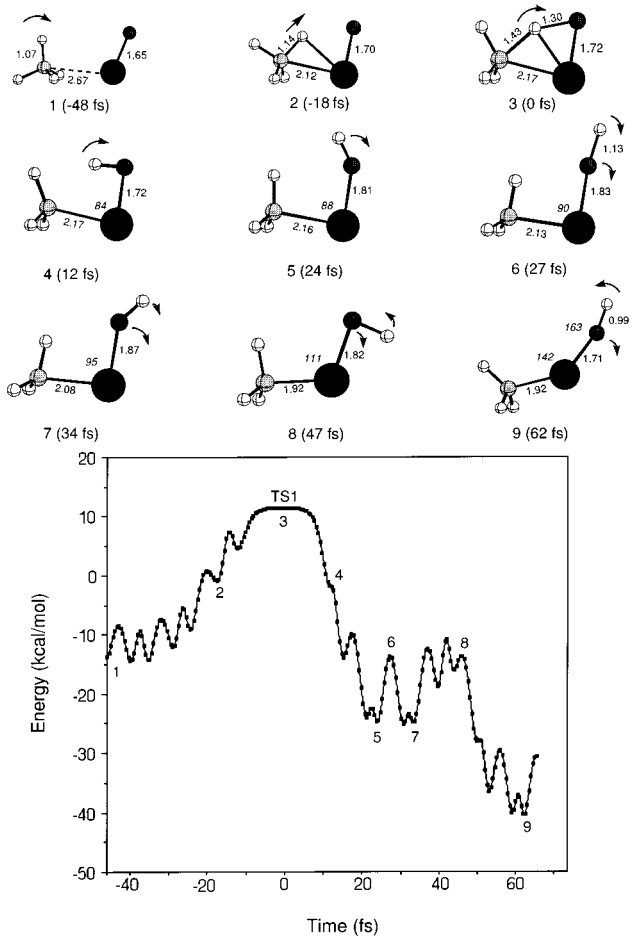


**Figure 1.** Dynamic reaction pathway for the concerted H atom abstraction of methane in the $FeO^+/CH_4$ system via the TS1 of the sextet state and snapshots of structures of the reacting system. The indicated relative energies are measured from the dissociation limit, $CH_4$ and $FeO^+$ ($^6\Sigma^+$). Bond distances indicated are in Å, and bond angles (italic) are in degrees. An initial kinetic energy of 0.1 kcal/mol was supplied to the TS1 toward both reactant and product directions.

is an important step for the activation of the C−H bonds of methane in the concerted mechanism. The reacting system reaches up to the TS1 and down to the hydroxy intermediate at about $t = 60$ fs. Thus, the concerted electronic process of the C−H bond dissociation and the O−H bond formation via the TS1 in the $FeO^+/CH_4$ system requires about 100 fs. Although it is difficult to strictly define the starting and the ending points due to the oscillating behavior of the potential energy, 100 fs is likely a typical value for the time required for the H atom abstraction in this concerted mechanism.

Changes in the distances of the C−H and the O−H bonds are shown along the dynamic reaction coordinate in Figure 2a. The oscillating behavior of the C−H and the O−H distances is clearly due to the molecular vibrations. Thus, the kinetic energy that the reacting system acquires in going down the slope of the potential energy surface is mainly partitioned into the C−H vibrational energy in the reactant complex and the O−H vibrational energy in the hydroxy intermediate. Changes in the Fe−O−H and the C−Fe−O angles are shown in Figure 2b. We see the oscillating behavior of the Fe−O−H angle; thus, the kinetic energy is in part partitioned into the Fe−O−H bending energy.

Let us next look at the H atom abstraction on the quartet potential energy surface; the quartet state of $FeO^+$ ($^4\Delta$) is only 6 kcal/mol above the ground state ($^6\Sigma^+$) in our DFT computa-

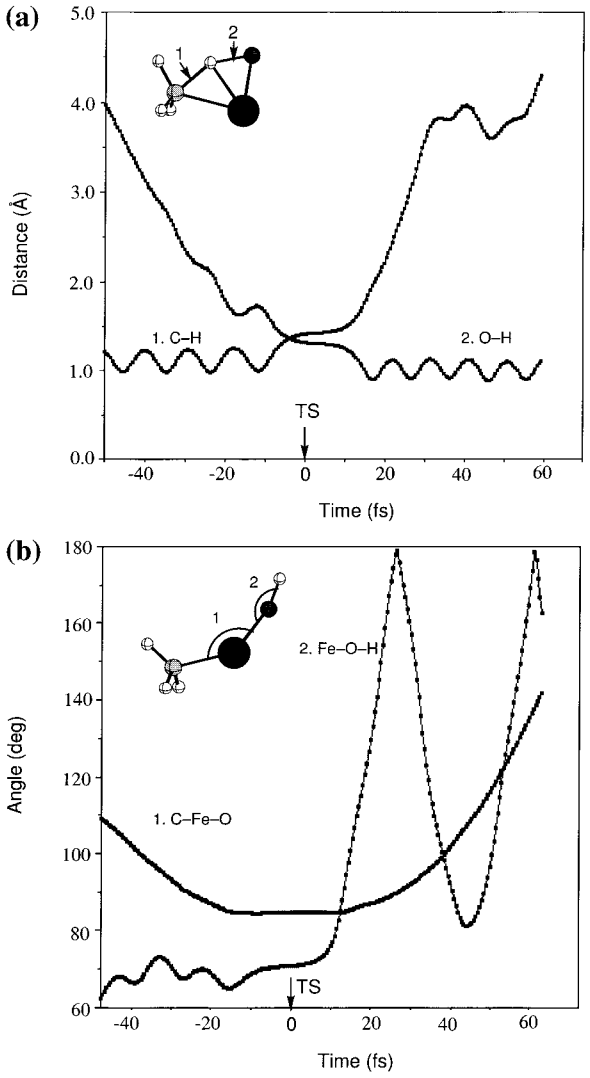


**Figure 2.** Changes in (a) the C−H and O−H bond distances and (b) the C−Fe−O and Fe−O−H bond angles along the dynamic reaction pathway for the H atom abstraction by the $FeO^+$ complex via the TS1 of the sextet state (see Figure 1).

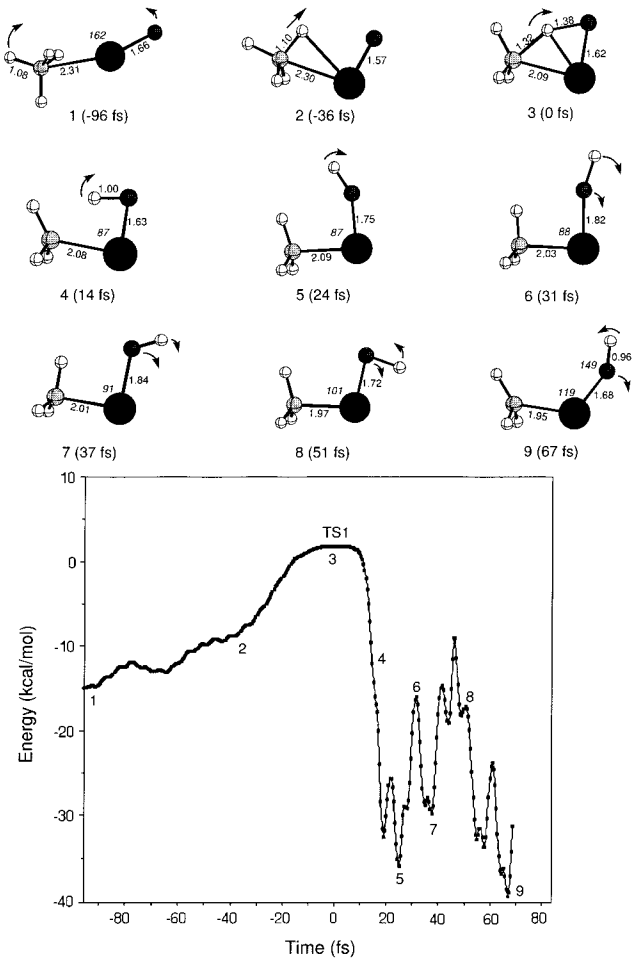


**Figure 3.** Dynamic reaction pathway for the concerted H atom abstraction of methane in the $FeO^+/CH_4$ system via the TS1 of the quartet state and snapshots of structures of the reacting system. The indicated relative energies are measured from the dissociation limit, $CH_4$ and $FeO^+$ ($^6\Sigma^+$). An initial kinetic energy of 0.1 kcal/mol was supplied to the TS1.

tions.[12b] Figure 3 presents a computed dynamic reaction pathway for the H atom abstraction of methane in the quartet state. Note that we measure the relative energy from a summation of the total energies of free methane and the $FeO^+$ complex of the ground state ($^6\Sigma^+$) as a standard. Thus, the barrier height of the TS1 in the quartet state is slightly higher than the initial potential energy that the reacting system possesses; we therefore expect that the quartet potential energy surface should provide a low-cost reaction pathway. The activation barrier for this step amounts to 15.7 kcal/mol when measured from the reactant complex. The spin inversion from the ground sextet state to the low-lying quartet state should therefore play an essential role in this reaction. General discussions on the so-called "two-state reactivity" have been given by Shaik et al.,[38] and computational results in the $FeO^+/CH_4$ system have been described in our previous papers.[12b,13] The reaction of the quartet state is likely to proceed slowly compared to that of the sextet state, while the general features of this reaction pathway are identical to those of Figure 1. This result arises from the restriction of our methodology. Because the total energy of the reacting system of the quartet state is smaller than that of the sextet state, the kinetic energy that the reacting system acquires on the quartet potential energy surface is smaller than that on the sextet potential energy surface. Accordingly, the reaction was computed to proceed slowly on the quartet potential energy surface under the initial condition that we assumed. Since the kinetic energy is not sufficient in the reactant pathway of the quartet state, it is not effectively partitioned into the C−H vibrational energy. The amplitude of the C−H vibrational energy is therefore not remarkable in Figure 3.

We next turn our attention to how the kinetic energy of the system is partitioned into vibrational modes along the dynamic reaction pathway for the H atom abstraction via TS1. Figure 4 shows changes in the amplitudes of normal coordinates along the dynamic reaction pathway before and after TS1 in the sextet state. The time-dependent equation for the normal coordinates[39] in the dynamics analysis can be written as

$$Q_i^{\mathrm{A}}(t) = \sum_k^{3N} (X_i(t+\Delta t) - X_k(t)) \sqrt{m_k} L_{ki}^{\mathrm{A}} \qquad (4)$$

in which $Q_i^{\mathrm{A}}$ is the $i$th normal coordinate, $X_k$ is the $k$th Cartesian coordinate, $m_k$ is the atomic mass corresponding to $X_k$, $L_{ki}^{\mathrm{A}}$ is the $k$th component of the $i$th normal mode of the equilibrium geometry, and $N$ is the number of atoms in the system. Here we took a time interval $\Delta t$ of 7.5 fs. As can be seen from Figure 4, the amplitude of each normal coordinate is small in the vicinity of TS1 and is significant near the reactant

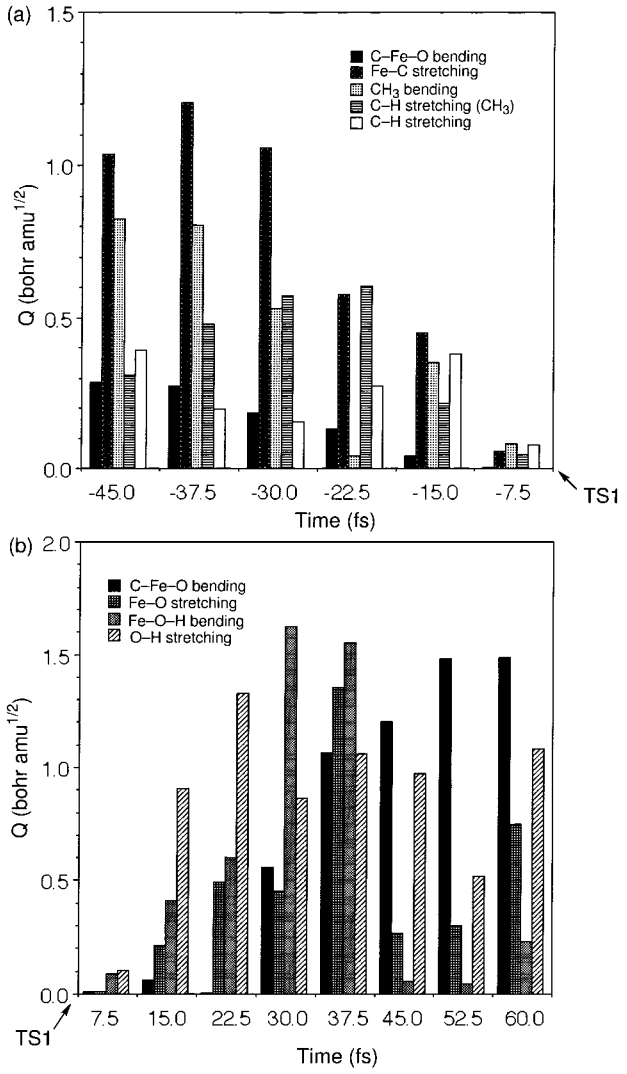


**Figure 4.** Changes in the amplitudes of normal coordinates along the dynamic reaction pathway for the concerted H atom abstraction of methane (a) before and (b) after TS1 in the sextet state.

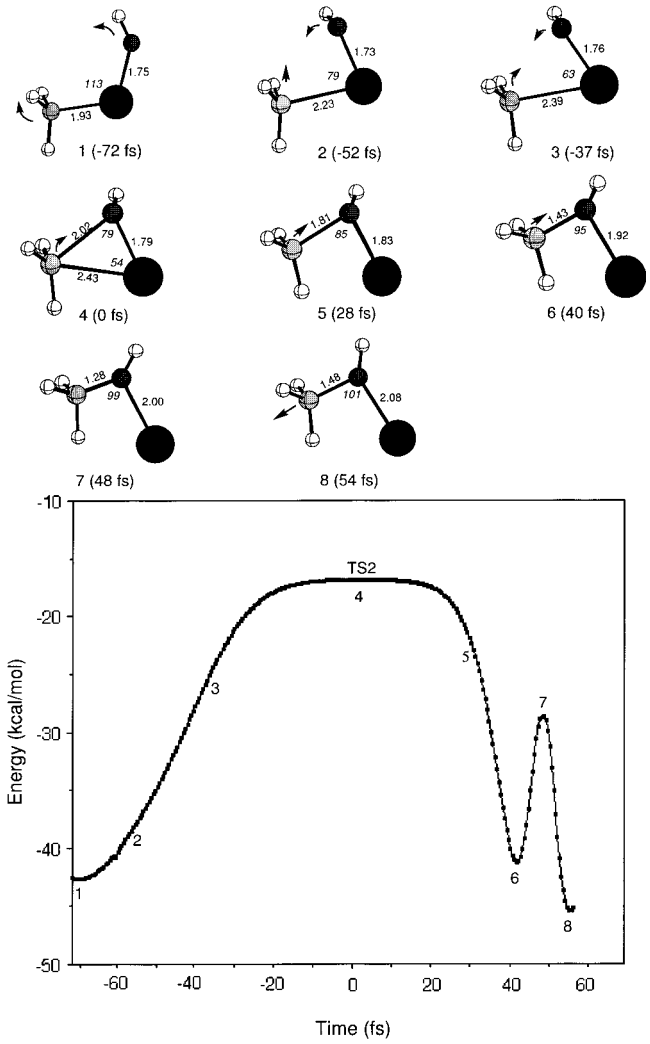


**Figure 5.** Dynamic reaction pathway for the methyl migration in the $FeO^+/CH_4$ system via the TS2 of the quartet state and snapshots of structures of the reacting system. The indicated relative energies are measured from the dissociation limit, $CH_4$ and $FeO^+$ ($^6\Sigma^+$). An initial kinetic energy of 0.1 kcal/mol was supplied to the TS2.

complex and the hydroxy intermediate because the system loses kinetic energy in going up the transition state. The stretching modes of the C−H bond and the O−H bond are enhanced before and after TS1, respectively. The amplitudes of these stretching modes are not significant, but their kinetic energies are greater than other modes of vibration because the force constants of these stretching modes are large compared to those of bending modes. The kinetic energy that the system acquires after passing TS1 is also partitioned into the Fe−O−H bending mode, the amplitude of which is very large at $t = 30$ fs. This is in good agreement with the fact that the angle of Fe−O−H is 180° at nearly $t = 30$ fs, as shown in Figure 2.

Having described the dynamic reaction pathway for the dissociation of the C−H bond of methane, let us next look at the second half of the reaction pathway indicated in Scheme 1. This reaction starts with the hydroxy intermediate and ends with the formation of the product (methanol) complex. Since the reacting system preferentially moves on the quartet energy surface in this region of the reaction pathway,[12b] we pay our attention to the reaction pathway of the quartet state. The transition state (TS2) has a three-centered structure associated with the methyl migration, the Fe−C distance being 2.43 Å and the C−O bond distance being 2.02 Å. The activation barrier for this step was predicted to be 28.6 kcal/mol when measured from the hydroxy intermediate. Figure 5 shows how the methyl migration occurs to lead to the product complex along the dynamic reaction coordinate of the quartet state. Starting from the hydroxy intermediate, the reacting system goes up to the TS2 and down to the product complex at about $t = 40$ fs. We see a jump of potential energy at $t = 48$ fs after the formation of the product complex. This intriguing phenomenon arises again from interconversion between the kinetic energy and the compressive energy of the C−O bond. The excess kinetic energy can be dissipated through nonradiative processes such as intramolecular vibrational energy redistribution (IVR)[40] even if the system has no interaction with external fields. IVR is an important relaxation process for hot molecules. When the system has various interactions with external fields, the energy can be dissipated through energy transfer to surroundings. If the energy is distributed by a solvent-assisted IVR process into low-energy vibrational modes, energy dissipation by the solvent should be a few picosecond process.

The sextet potential energy profile along the dynamic reaction pathway for the methyl migration is essentially identical to the quartet one. The reader can see the dynamic reaction pathway of the sextet state in Supporting Information. Since the sextet potential energy surface lies about 10 kcal/mol above the quartet surface, the methyl migration should take place preferentially

**SCHEME 5**

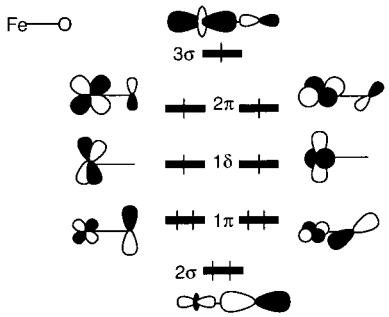


on the quartet potential energy surface. In fact, the activation barrier for this step was computed to be 36.2 kcal/mol in the sextet state and 28.6 kcal/mol in the quartet state.[12b] In this way, we conclude that the quartet potential energy surface should play an essential role in the methane−methanol conversion in the $FeO^+/CH_4$ system with respect to both the H atom abstraction and the methyl migration.

**Direct H Atom Abstraction of Methane.** We next address a widely believed radical mechanism called the oxygen rebound mechanism,[14,15] in which a direct H atom abstraction from the substrate is assumed to take place in the initial stages of enzymatic (especially cytochrome P450-catalyzed) hydrocarbon hydroxylations. This mechanism is in remarkable contrast to the concerted mechanism via the four-centered transition state (TS1) discussed above in that the Fe ion plays no significant role in this radical process while it is a major contributor in the concerted process. Siegbahn and Crabtree and Basch et al.[20] have proposed from DFT computations that the direct H atom abstraction should take place in the nonet and higher-spin states in diiron model complexes of soluble MMO following this radical mechanism. This type of H atom abstraction occurs via a nearly linear C−H−O(Fe) transition state (TSd), as indicated in Scheme 3. Since determining the mechanism of catalytic and enzymatic C−H bond dissociation is of current interest, making a comparison between the concerted and the direct H atom abstractions is a very interesting subject. We thus decided to compare the femtosecond dynamic behavior of the two different mechanisms. In this subsection, we consider the dynamics of the direct H atom abstraction of methane by the $FeO^+$ complex.

As indicated in our previous paper,[12c] the direct H atom abstraction of methane occurs via a linear transition state only in the high-spin sextet state of $FeO^+$. Despite our best efforts, such a transition state was not found in the low-spin quartet state of the $FeO^+/CH_4$ system. This computational result may be reasonable in view of the frontier orbitals of $FeO^+$ in Scheme 5 because the $3\sigma$ orbital of $FeO^+$, the amplitude of which exists on the oxygen atom in some degree, is singly occupied in the sextet state and it plays a major role in the direct H atom abstraction. However, this $3\sigma$ orbital is vacant in the low-spin quartet state, and therefore the spin density on the oxygen atom is significantly diminished in the low-spin quartet state. In fact, computed spin densities of the oxygen atom are +1.14 and −0.63 in the sextet ($^6\Sigma^+$) and the quartet ($^4\Delta$) states, respectively. As a result, the direct H atom abstraction is reasonably computed not to occur in the low-spin quartet state.

The partially filled $2\pi$ set should also play a role in the direct abstraction; this is conceivable from the fact that the optimized transition state is considerably bent with respect to the Fe−O−H angle.[12c] However, the $1\delta$ set has no contribution to the direct H atom abstraction because the $1\delta$ has no orbital amplitude on the oxygen atom, due to orbital symmetry restriction. We therefore conclude that a requisite precondition

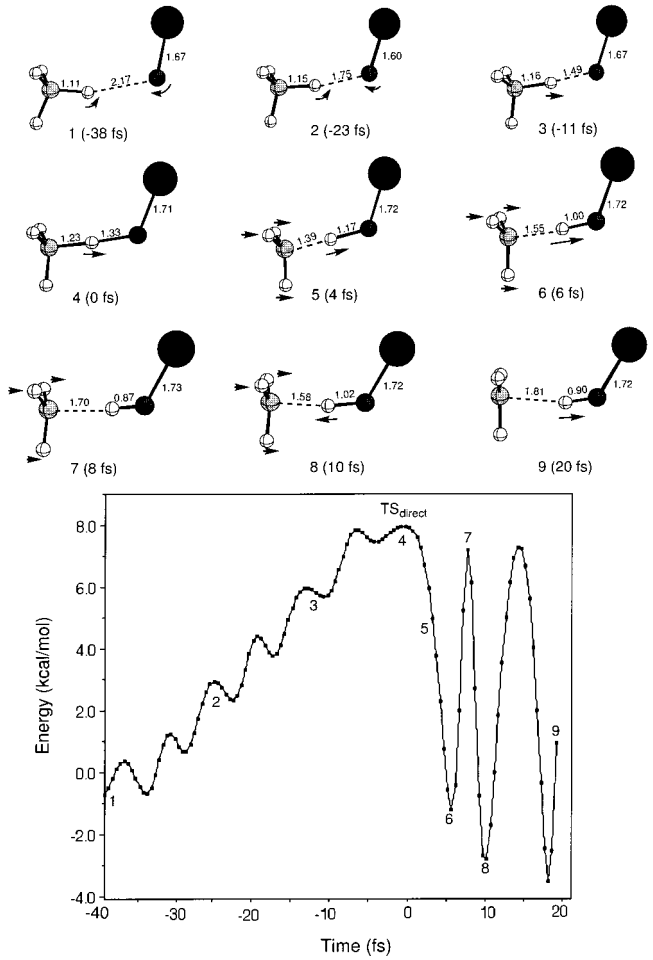


**Figure 6.** Dynamic reaction pathway for the direct H atom abstraction of methane in the $FeO^+/CH_4$ system via the TSd of the sextet state and snapshots of structures of the reacting system. The indicated relative energies are measured from the dissociation limit, $CH_4$ and $FeO^+$ ($^6\Sigma^+$). An initial kinetic energy of 1 kcal/mol was supplied to the transition state.

for the direct H atom abstraction is that the $3\sigma$ orbital of $FeO^+$ is singly occupied. Thus, the radical character of the oxo species is important for the direct abstraction. The computed spin density of the oxygen atom of $FeO^+$ is 1.14 in the sextet state, but the reader should note that the total spin density is partitioned into $\sigma$ and $\pi$ components. The $\sigma$ spin density, which can play an essential role in the direct abstraction, is about 0.4; therefore, contrary to our expectation, the $\sigma$ radical character of the oxo species is not so significant as we expect. This is the reason that the transition state for the direct abstraction was predicted to lie 4 kcal/mol above the TS1 of the quartet state.[12c] Moreover, we think that the existence of the Fe−C bond in the four-centered TS1 should contribute to the preference of the two-step concerted mechanism in the $FeO^+/CH_4$ system.

The transition state was predicted at the C−H bond distance of 1.23 Å and at the O−H bond distance of 1.33 Å. We present in Figure 6 a computed dynamic reaction pathway for the direct H atom abstraction by the oxo moiety of the $FeO^+$ complex and femtosecond snapshots of the structures of the system as a function of time. The system reaches up to the linear transition state and down to the dissociation into the $Fe^+OH$ species and the $CH_3$ radical species at $t = 6$ fs. Thus, this direct H atom abstraction is faster than the concerted H atom abstraction discussed above. Note that the formed methyl radical becomes nearly planar at about $t = 20$ fs, indicating that the H atom

abstraction is completely finished. If this methyl radical is not bound, we can expect an inversion of configuration at the methyl carbon to occur, but this carbon radical is not completely free from the metal complex. It would be interesting to see whether such a bound carbon radical species can undergo an inversion of configuration in transition-metal catalyzed reactions.

The oscillating behavior in the potential energy profile prior to the transition state is clearly ascribed to the C−H bond vibration of the methane molecule. We see a jump of potential energy at $t = 8$ fs after the O−H bond is formed, which arises from transformation of the kinetic energy to the compressive energy of the O−H bond. We see from the significant oscillating behavior that the interconversion between the kinetic energy and the O−H compressive energy continues because the system is isolated.

The result presented above was obtained when the initial kinetic energy of 1 kcal/mol was given to the transition state toward both reactant and product valleys. However, when we supplied an initial kinetic energy of 10 kcal/mol, the H atom once abstracted by the oxo species came back to the methyl radical to form the methane molecule again. Such a strange phenomenon can occur in an isolated system because the excess kinetic energy that is partitioned into a local vibrational mode is not effectively dissipated to external fields in our calculations.

### Isotope Effects for H Atom Abstractions of Methane

The kinetic isotope effect $k_H/k_D$ is an important measure in discussing how the electronic process for H atom abstraction of substrate hydrocarbon takes place in catalytic and enzymatic reactions. Such measurements have been extensively performed in mechanistic investigations of hydrocarbon hydroxylations by cytochrome P450.[14,15] In this section, we consider the isotope effects on the time required for our concerted H atom abstraction via the TS1 and for the direct H atom abstraction via the linear transition state. Direct comparison of the real-time analysis for the two kinds of H atom abstraction is of great importance in discussing how H atom abstraction takes place.

We first look at the H/D isotope effects on the concerted hydrogen atom abstraction via the four-centered transition state (TS1). Figure 7 shows a computed potential energy profile for the deuterium (D) atom abstraction in the $FeO^+/CD_4$ system via the TS1 along the dynamic reaction coordinate of the quartet state. We presented a corresponding energy profile for the H atom abstraction in Figure 3. The potential energy profiles in Figures 3 and 7 are, of course, essentially identical because of the analysis performed within the framework of the Born−Oppenheimer approximation, but the time scales in Figures 3 and 7 are clearly different, due to the difference in mass.

A computed dynamic reaction pathway for the D atom abstraction via the TS1 in the $FeO^+/CD_4$ system of the sextet state can be seen in Supporting Information. The general features of this dynamic reaction pathway are identical to those in Figure 1. We thus do not repeat similar discussions here. The D atom abstraction is finished in 130−140 fs.

Let us next look at the H/D isotope effect on the direct hydrogen atom abstraction that occurs via the linear transition state (TSd). As mentioned earlier, this reaction occurs only on the high-spin sextet potential energy surface. We thus ran the dynamics calculations on the sextet potential energy surface. The reacting system goes up to the linear transition state and down to the dissociation into the $Fe^+OH$ species and the $CH_3$ radical species at $t = 9$ fs, as shown in Figure 8. Then the methyl radical finally becomes planar at $t = 25$ fs.

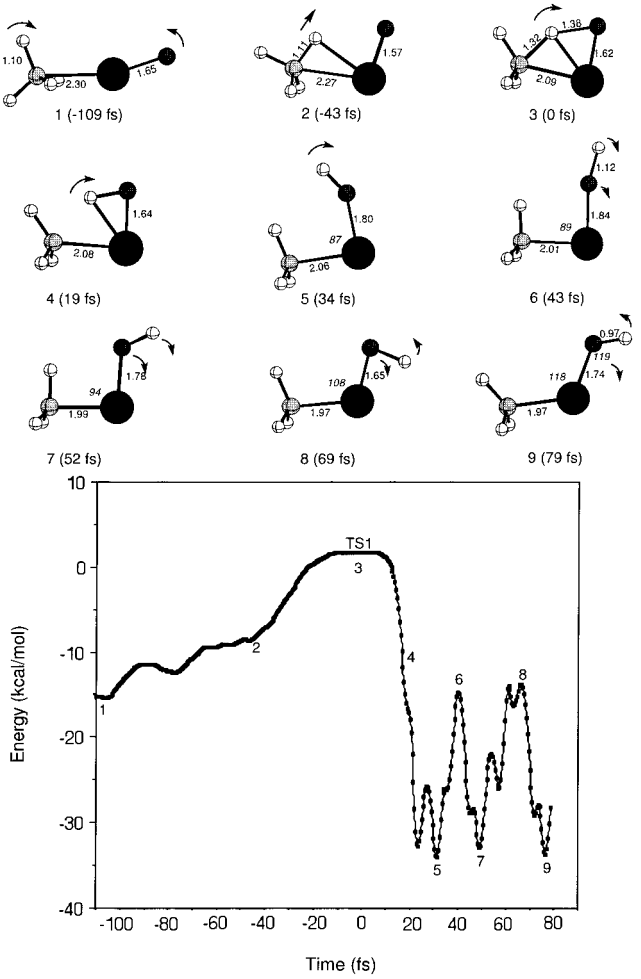


**Figure 7.** Dynamic reaction pathway for the concerted D atom abstraction of deuteriomethane in the $FeO^+/CD_4$ system via the TS1 of the quartet state and snapshots of structures of the reacting system. The indicated relative energies are measured from the dissociation limit, $CH_4$ and $FeO^+$ ($^6\Sigma^+$). An initial kinetic energy of 0.1 kcal/mol was supplied to the TS1.

Having described the isotope effects on the real-time analysis for the concerted and the direct H(D) atom abstractions, we next address the kinetic isotope effects ($k_H/k_D$), which can be calculated with the transition-state theory.[41] The values of $k_H/k_D$ were obtained from the following expression.[28]

$$\frac{k_{CH_4}}{k_{CD_4}} = \left(\frac{m^R_{CD_4} m^{\#}_{CH_4}}{m^R_{CH_4} m^{\#}_{CD_4}}\right)^{3/2} \left(\frac{I_{CD_4}}{I_{CH_4}}\right)^{3/2} \times \left(\frac{I^{\#}_{xCH_4} I^{\#}_{yCH_4} I^{\#}_{zCH_4}}{I^{\#}_{xCD_4} I^{\#}_{yCD_4} I^{\#}_{zCD_4}}\right)^{1/2} \frac{q^R_{\nu CH_4} q^{\#}_{\nu CH_4}}{q^R_{\nu CH_4} q^{\#}_{\nu CD_4}} \exp\left(-\frac{E^{\#}_{CH_4} - E^{\#}_{CD_4}}{RT}\right) \quad (5)$$

where superscripts R and # specify the reactant methane and the transition state, respectively, for the molecular mass $m$, the moment of inertia $I$, the vibrational partition function $q$, and the activation energy $E$. The last exponential term is dominant in this equation because the other terms can be almost all canceled between denominators and numerators. The numerator in the last exponential term comes from the fact that C−H dissociation has a lower activation energy than C−D dissociation on account of the former's greater zero-point vibrational energy.

Table 1 summarizes computed values of $k_H/k_D$ for the concerted abstraction via TS1 of the sextet and the quartet states

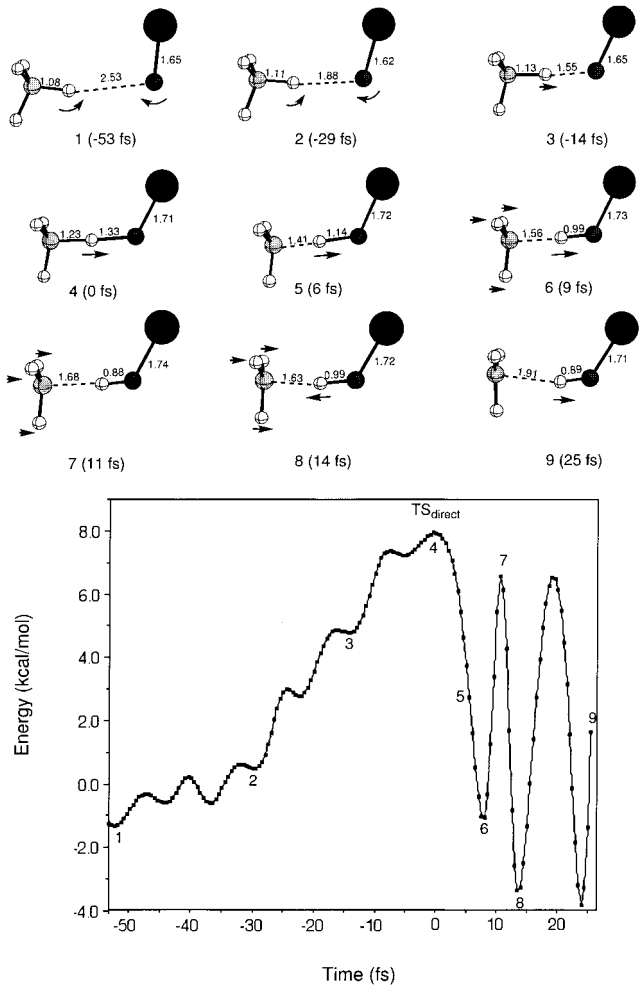


**Figure 8.** Dynamic reaction pathway for the direct D atom abstraction of deuteriomethane in the $FeO^+/CD_4$ system via the TSd of the sextet state and snapshots of structures of the reacting system, $CH_4$ and $FeO^+$ ($^6\Sigma^+$). An initial kinetic energy of 1 kcal/mol was supplied to the transition state.

**TABLE 1: Computed Values of the Kinetic Isotope Effects ($k_H/k_D$) in the H(D) Atom Abstractions in the $FeO^+/CH(D)_4$ System via TS1 and TSd as a Function of Temperature**

| $T$ (K) | TS1(sextet) | TS1(quartet) | TSd(sextet) |
|---|---|---|---|
| 200 | 19.55 | 16.74 | 40.60 |
| 250 | 13.00 | 11.56 | 23.62 |
| 300 | 9.68 | 8.82 | 16.07 |
| 350 | 7.67 | 7.11 | 11.96 |
| 400 | 6.34 | 5.96 | 9.40 |

and for the direct abstraction via TSd of the sextet state in the $FeO^+/CH(D)_4$ system as a function of temperature. At 300 K, the value for the concerted abstraction is 9.68 and 8.82 in the sextet and the quartet states, respectively, and that for the direct abstraction in the sextet state is 16.07. The predicted isotope effect is more significant in the direct abstraction than in the concerted abstraction, as expected. But the concerted mechanism gives rather large isotope effects. From a $^3$H NMR analysis, Floss, Lipscomb, and their collaborators[42] obtained a value of $4.2 \pm 0.2$ for an intramolecular primary kinetic isotope effect for hydrogen abstraction by sMMO, thus suggesting that the reaction may not be concerted. The kinetic isotope effects for P450-catalyzed hydrocarbon hydroxylations give larger $k_H/k_D$ values, but it is rare that observed $k_H/k_D$ values exceed 15 (see refs 15). Therefore, it is impossible to determine from measured kinetic isotope effects which of our concerted mechanism and the oxygen rebound mechanism is more appropriate.

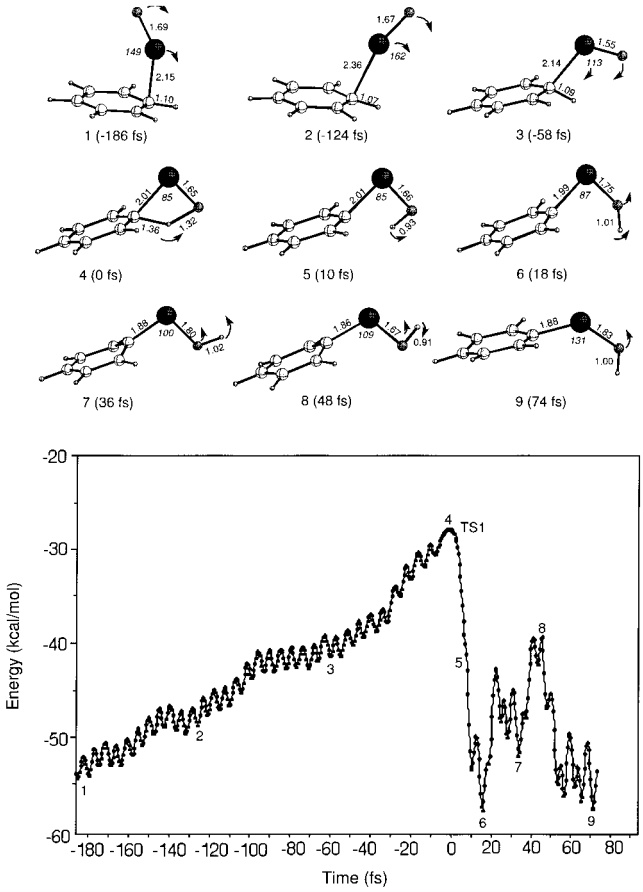


**Figure 9.** Dynamic reaction pathway for the concerted H atom abstraction of benzene in the $FeO^+/C_6H_6$ system via the TS1 of the quartet state and snapshots of structures of the reacting system. The indicated relative energies are measured from the dissociation limit, $C_6H_6$ and $FeO^+$ ($^4\Delta$). Bond distances indicated are in Å, and bond angles (italic) are in degrees. An initial kinetic energy of 1 kcal/mol was supplied to the TS1 toward both reactant and product directions.

## Benzene−Phenol Conversion

In this section we turn our attention to the femtosecond dynamic reaction pathway for the direct conversion of benzene to phenol by the $FeO^+$ complex. Determining how this reaction takes place is of great use from the technological viewpoint because of a demand for the direct process of the benzene−phenol conversion.[21b] Detailed descriptions of the reaction intermediates and the transition states as well as of the energetics in the benzene−phenol conversion by $FeO^+$ can be seen in our recent paper.[25] The general profile of the reaction pathway is quite similar to that of the methane−methanol conversion with respect to the H atom abstraction (TS1) as well as of the phenyl migration (TS2), as indicated earlier in Schemes 1 and 2.

Since in this reaction the low-spin quartet potential energy surface plays a dominant role to provide a low-lying reaction pathway,[25] which is slightly different from the methane hydroxylation, we computed only the dynamic reaction pathway on the quartet potential energy surface. We present in Figure 9 a computed potential energy profile for the C−H bond dissociation of benzene in the $FeO^+/C_6H_6$ system. The four-centered TS1 of the quartet state was predicted at the C−H bond distance of 1.36 Å and at the O−H bond distance of 1.32 Å. This reaction also starts with the formation of the reactant

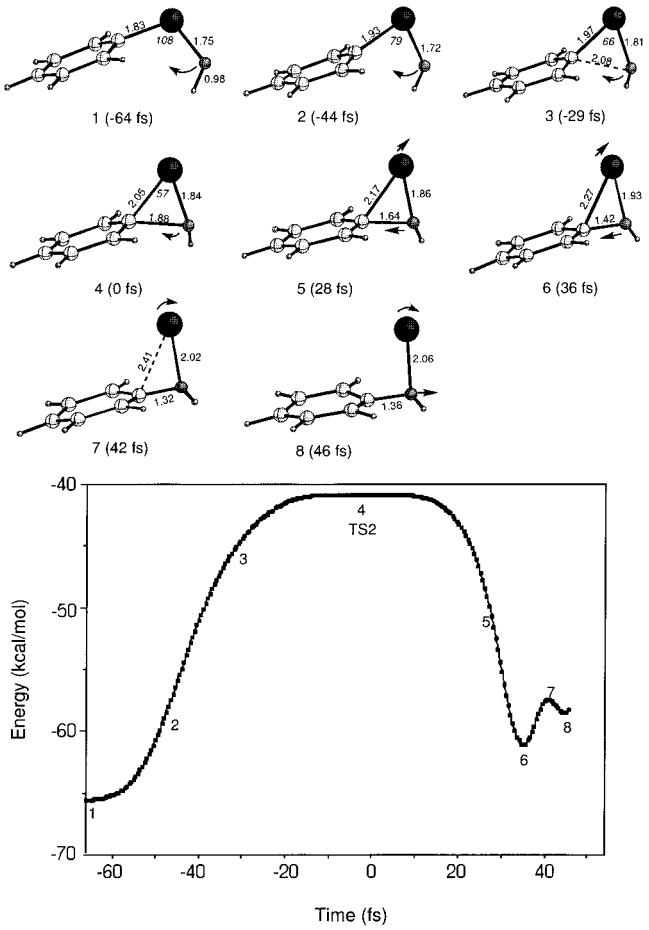


**Figure 10.** Dynamic reaction pathway for the phenyl migration in the $FeO^+/C_6H_6$ system via the TS2 of the quartet state and snapshots of structures of the reacting system. The indicated relative energies are measured from the dissociation limit, $C_6H_6$ and $FeO^+$ ($^4\Delta$). An initial kinetic energy of 1 kcal/mol was supplied to the TS2 toward both reactant and product directions.

(benzene) complex and ends with the hydroxy intermediate ($HO-Fe^+-C_6H_5$). The reactant complex thus formed in the initial stages of the reaction is a $\pi$ complex, not a $\sigma$ complex. The binding energy of the $OFe^+(C_6H_6)$ complex with an $\eta^2$-binding mode is large compared to that of the methane complex because of the good interaction between the benzene HOMO and the $1\delta$ and the $2\pi$ orbitals of the bare $FeO^+$ complex.[25]

As can be seen in Figure 9, the reaction pathway for the C−H bond dissociation of benzene is extraordinarily long and the movement of the oxo species is significant, but it was confirmed from this dynamics analysis that this electronic process is a single-step reaction via a single transition state (TS1). We show from the dynamics analysis that the system goes up to the TS1 and the H atom abstraction of benzene requires about 200 fs to be completed. The reader can see how long the reaction pathway is with respect to this H atom abstraction as compared to the H atom abstraction in the $FeO^+/CH_4$ case. The indicated relative energy is measured from the dissociation limit of the reactants, i.e., $C_6H_6$ and $FeO^+$ ($^4\Delta$). Since the binding energy between benzene and the $FeO^+$ complex is quite large (~60 kcal/mol), the barrier height for the TS1 looks very high when measured from the reactant complex. However, the potential energy of the TS1 in the $FeO^+/C_6H_6$ system lies well below the dissociation limit, suggesting that the H atom abstraction of benzene should take place easily. In contrast, the binding energy between methane and the $FeO^+$ complex is approximately 20 kcal/mol, and so the barrier height for the TS1 does not look very high when measured from the reactant complex. However, the potential energy of the TS1 in the $FeO^+/CH_4$ case is slightly higher than that of the dissociation limit. This fact shows a striking difference in the reactivities of methane and benzene. Therefore, the reactivity of $FeO^+$ toward methane is likely to be lower than that toward benzene.

The oscillating behavior before and after the TS1 in Figure 9 is again due to the C−H vibration of the benzene molecule and the O−H vibration, respectively. Thus, the kinetic energy that the system acquires in going down the potential energy surface is mainly partitioned into the C−H vibrational energy in the reactant complex and the O−H vibrational energy in the hydroxy intermediate. Femtosecond snapshots of the structures of the system show that the iron and the oxygen atoms move significantly along the dynamic reaction coordinate of this single-step reaction. As can be seen from snapshots 5−8 in Figure 9, the Fe−O−H bending motion is also remarkable after passing over the TS1.

The second half of the benzene−phenol conversion starts with the hydroxy intermediate and ends with the formation of the product (phenol) complex, as shown in Figure 10. This concerted electronic process can be viewed as a phenyl migration or an OH migration. The transition state (TS2) is a typical, three-centered structure at the Fe−C distance of 2.05 Å and at the C−O bond distance of 1.88 Å in the quartet state. The activation barrier for the TS2 was predicted to be 28.7 kcal/mol.[25] The time required for the chemical processes of the C−O bond formation and the Fe−C bond dissociation was computed to be about 100 fs. From our experience gained in this study, 100 fs is likely a typical time scale for bond formations and dissociations catalyzed by transition-metal complexes, except for the C−H bond dissociation of benzene, which requires about 200 fs.

## Conclusions

We performed femtosecond dynamics analyses on the methane−methanol conversion by the bare iron−oxo complex ($FeO^+$) using the B3LYP density-functional-theory (DFT) method. The dynamic behavior of the reaction intermediates and the transition states along the two-step concerted reaction pathway in Scheme 1 was discussed in detail. The concerted H atom abstraction via the four-centered transition state (TS1) and the direct H atom abstraction via the transition state with the linear C−H−O(Fe) array (TSd) were investigated on the sextet and the quartet potential energy surfaces of the $FeO^+/CH_4$ system. The concerted H atom abstraction is slightly preferred in energy to the direct H atom abstraction, due to the existence of the Fe−C bond in the concerted transition state (TS1). The two-step, concerted H atom abstraction and methyl migration lead to the conversion of methane to methanol. We demonstrated that both the concerted H atom abstraction and the methyl migration occur in a time scale of 100 fs in the concerted mechanism. The isotope effects of the concerted and the direct H(D) atom abstractions in the $FeO^+/CH_4$ system were also computed and analyzed. Predicted values of the kinetic isotope effect ($k_H/k_D$) for H(D) atom abstraction are about 9 in the concerted mechanism and about 16 in the direct abstraction mechanism at 300 K. Dynamics calculations were also carried out on the direct benzene−phenol conversion by the $FeO^+$ complex. The general profile of the benzene−phenol conversion is identical to that of the methane−methanol conversion with respect to essential bonding characters; the two-step, concerted H atom abstraction and phenyl migration lead to the conversion

of benzene to phenol. We also demonstrated that the concerted H atom abstraction occurs in 200 fs and the phenyl migration occurs in 100 fs. The reaction pathway for the C−H bond dissociation of benzene is extraordinarily long, but it was confirmed from a dynamics analysis that this process is a single-step reaction via a single transition state (TS1).

**Acknowledgment.** K.Y. is grateful for a Grant-in-Aid for Scientific Research on the Priority Area "Molecular Biometallics" from the Ministry of Education, Science, Sports, and Culture of Japan in support of this work. Thanks are also due to the Institute for Fundamental Chemistry for its support through the "Research for the Future" Program from the Japan Society for the Promotion of Science (JSPS-RFTF96P00206). Y.S. thanks the JSPS for a graduate fellowship. Computational time was provided by the Supercomputer Laboratory of Kyoto University and by the Computer Center of the Institute for Molecular Science.

**Supporting Information Available:** Figures of the dynamic reaction pathways. This material is available free of charge via the Internet at http://pubs.acs.org.

## References and Notes

(1) (a) Shilov, A. E. *The Activation of Saturated Hydrocarbons by Transition Metal Complexes*; Reidel: Dortrecht, The Netherlands, 1984. (b) Shilov, A. E. *Metal Complexes in Biomimetic Chemical Reactions*; CRC: Boca Raton, FL, 1996.

(2) (a) Bergman, R. G. *Science* **1984**, *223*, 902. (b) Arndtsen, B. A.; Bergman, R. G.; Mobley, T. A.; Peterson, T. H. *Acc. Chem. Res.* **1995**, *28*, 154.

(3) *Activation and Functionalization of Alkanes*; Hill, C. L. Ed.; Wiley: New York, 1989.

(4) Davies, J. A.; Watson, P. L.; Liebman, J. F.; Greenberg, A. *Selective Hydrocarbon Activation*; VCH: New York, 1990.

(5) (a) Crabtree, R. H. *Chem. Rev.* **1985**, *85*, 245. (b) Crabtree, R. H. *Chem. Rev.* **1995**, *95*, 987.

(6) Gesser, H. D.; Hunter, N. R.; Prakash, C. B. *Chem. Rev.* **1985**, *85*, 237.

(7) Lunsford, J. H. *Angew. Chem., Int. Ed. Engl.* **1995**, *34*, 970.

(8) Schneider, J. J. *Angew. Chem., Int. Ed. Engl.* **1996**, *35*, 1068.

(9) Hall, C.; Perutz, R. N. *Chem. Rev.* **1996**, *96*, 3125.

(10) (a) Schröder, D.; Schwarz, H. *Angew. Chem., Int. Ed. Engl.* **1990**, *29*, 1433. (b) Schröder, D.; Fiedler, A.; Hrusák, J.; Schwarz, H. *J. Am. Chem. Soc.* **1992**, *114*, 1215. (c) Schröder, D.; Schwarz, H.; Clemmer, D. E.; Chen, Y.-M.; Armentrout, P. B.; Baranov, V. I.; Böhme, D. K. *Int. J. Mass Spectrom. Ion Processes* **1997**, *161*, 175.

(11) Review: Schröder, D.; Schwarz, H. *Angew. Chem., Int. Ed. Engl.* **1995**, *34*, 1973.

(12) (a) Yoshizawa, K.; Shiota, Y.; Yamabe, T. *Chem. Eur. J.* **1997**, *3*, 1160. (b) Yoshizawa, K.; Shiota, Y.; Yamabe, T. *J. Am. Chem. Soc.* **1998**, *120*, 564. (c) Yoshizawa, K.; Shiota, Y.; Yamabe, T. *Organometallics* **1998**, *17*, 2825.

(13) Yoshizawa, K.; Shiota, Y.; Yamabe, T. *J. Chem. Phys.* **1999**, *111*, 538.

(14) Groves, J. T. *J. Chem. Educ.* **1985**, *62*, 928.

(15) See for example: (a) *Cytochrome P450: Structure, Mechanism, and Biochemistry*, 2nd ed.; Ortiz de Montellano, P. R., Ed.; Plenum: New York, 1995. (b) Sono, M.; Roach, M. P.; Coulter, E. D.; Dawson, J. H. *Chem. Rev.* **1996**, *96*, 2841.

(16) Recent reviews on sMMO: (a) Wallar, B. J.; Lipscomb, J. D. *Chem. Rev.* **1996**, *96*, 2625. (b) Que, L., Jr.; Dong, Y. *Acc. Chem. Res.* **1996**, *29*, 190. (c) Kurtz, D. M., Jr. *J. Biol. Inorg. Chem.* **1997**, *2*, 159. (d) Andersson, K. K.; Gräslund, A. *Adv. Inorg. Chem.* **1995**, *43*, 359. (e) Feig, A. L.; Lippard, S. J. *Chem. Rev.* **1994**, *94*, 759. (f) Lipscomb, J. D. *Annu. Rev. Microbiol.* **1994**, *48*, 371. (g) Lippard, S. J. *Angew. Chem., Int. Ed. Engl.* **1988**, *27*, 344.

(17) (a) Yoshizawa, K. *J. Biol. Inorg. Chem.* **1998**, *3*, 318. (b) Yoshizawa, K.; Yamabe, T.; Hoffmann. R. *New J. Chem.* **1997**, *21*, 151. (c) Yoshizawa, K.; Ohta, T.; Yamabe, T.; Hoffmann, R. *J. Am. Chem. Soc.* **1997**, *119*, 12311. (d) Yoshizawa, K.; Ohta, T.; Yamabe, T. *Bull. Chem. Soc. Jpn.* **1998**, *71*, 1899. (e) Yoshizawa, K.; Suzuki, A.; Shiota, Y.; Yamabe, T. *Bull. Chem. Soc. Jpn.*, in press. (f) Yoshizawa, K. *J. Inorg. Biochem.* **2000**, *78*, 23.

(18) Shu, L.; Nesheim, J. C.; Kauffmann, K.; Münck, E.; Lipscomb, J. D.; Que, L., Jr. *Science* **1997**, *275*, 515.

(19) Commentaries on the mechanism of sMMO: (a) Deeth, R. J.; Dalton, H. *J. Biol. Inorg. Chem.* **1998**, *3*, 302. (b) Whittington, D. A.; Valentine, A. M.; Lippard, S. J. *J. Biol. Inorg. Chem.* **1998**, *3*, 307. (c) Siegbahn, P. E. M.; Crabtree, R. H.; Nordlund, P. *J. Biol. Inorg. Chem.* **1998**, *3*, 314. (d) Yoshizawa, K. *J. Biol. Inorg. Chem.* **1998**, *3*, 318. (e) Shteinman, A. A. *J. Biol. Inorg. Chem.* **1998**, *3*, 325. (f) Lipscomb, J. D.; Que, L., Jr. *J. Biol. Inorg. Chem.* **1998**, *3*, 331.

(20) (a) Siegbahn, P. E. M.; Crabtree, R. H. *J. Am. Chem. Soc.* **1997**, *119*, 3103. (b) Siegbahn, P. E. M. *Inorg. Chem.* **1999**, *38*, 2880. (c) Basch, H.; Mogi, K.; Musaev, D. G.; Morokuma, K. *J. Am. Chem. Soc.* **1999**, *121*, 7249.

(21) See for example: (a) Morrison, R. T.; Boyd, R. N. *Organic Chemistry*, 6th ed.; Prentice Hall: New York, 1992; p 893. (b) *Chem. Eng. News* **1998**, April 6, 21.

(22) Iwamoto, M.; Hirata, J.; Matsukami, K.; Kagawa, S. *J. Phys. Chem.* **1983**, *87*, 665.

(23) (a) Panov, G. I.; Sheveleva, G. A.; Kharitonov, A. S.; Romannikov, V. N.; Vostrikova, L. A. *Appl. Catal. A: General* **1992**, *82*, 31. (b) Panov, G. I.; Kharitonov, A. S.; Sobolev, V. I. *Appl. Catal. A: General* **1993**, *98*, 1.

(24) (a) Schröder, D.; Schwarz, H. *Helv. Chim. Acta* **1992**, *75*, 1281. (b) Becker, H.; Schröder, D.; Zummack, W.; Schwarz, H. *J. Am. Chem. Soc.* **1994**, *116*, 1096.

(25) Yoshizawa, K.; Shiota, Y.; Yamabe, T. *J. Am. Chem. Soc.* **1999**, *121*, 147.

(26) (a) Newcomb, M.; Le Tadic-Biadatti, M. H.; Chestney, D. L.; Roberts, E. S.; Hollenberg, P. F. *J. Am. Chem. Soc.* **1995**, *117*, 12085. (b) Choi, S. Y.; Eaton, P. E.; Hollenberg, P. F.; Liu, K. E.; Lippard, S. J.; Newcomb, M.; Putt, D. A.; Upadhyaya, S. P.; Xiong, Y. *J. Am. Chem. Soc.* **1996**, *118*, 6547. (c) Toy, P. H.; Dhanabalasingam, B.; Newcomb, M.; Hanna, I. H.; Hollenberg, P. F. *J. Org. Chem.* **1997**, *62*, 9114.

(27) Hamilton, G. A. In *Molecular Mechanisms of Oxygen Activation*; Hayaishi, O. Ed.; Academic: New York, 1974.

(28) Filatov, M.; Shaik, S. *J. Phys. Chem. A* **1998**, *102*, 3835.

(29) (a) Becke, A. D. *Phys. Rev.* **1988**, *A38*, 3098. (b) Becke, A. D. *J. Chem. Phys.* **1993**, *98*, 5648.

(30) Lee, C.; Yang, W.; Parr, R. G. *Phys. Rev.* **1988**, *B37*, 785.

(31) Vosko, S. H.; Wilk, L.; Nusair, M. *Can. J. Phys.* **1980**, *58*, 1200.

(32) Wachters, A. J. H. *J. Chem. Phys.* **1970**, *52*, 1033.

(33) Raghavachari, K.; Trucks, G. W. *J. Chem. Phys.* **1989**, *91*, 1062.

(34) Krishnan, R.; Binkley, J. S.; Seegar, R.; Pople, J. A. *J. Chem. Phys.* **1980**, *72*, 650.

(35) Dunning, T. H.; Hay, P. J. In *Modern Theoretical Chemistry*; Schaefer, H. F., Ed.; Plenum: New York, 1976.

(36) Frisch, M. J.; Trucks, G. W.; Schlegel, H. B.; Gill, P. M. W.; Johnson, B. G.; Robb, M. A.; Cheeseman, J. R.; Keith, T. A.; Petersson, G. A.; Montgomery, J. A.; Raghavachari, K.; Al-Laham, M. A.; Zakrzewski, V. G.; Ortiz, J. V.; Foresman, J. B.; Cioslowski, J.; Stefanov, B. B.; Nanayakkara, A.; Challacombe, M.; Peng, C. Y.; Ayala, P. Y.; Chen, W.; Wong, M. W.; Andres, J. L.; Replogle, E. S.; Gomperts, R.; Martin, R. L.; Fox, D. J.; Binkley, J. S.; Defrees, D. J.; Baker, J.; Stewart, J. J. P.; Head-Gordon, M.; Gonzalez, C.; Pople, J. A. *Gaussian 94*; Gaussian Inc.: Pittsburgh, PA, 1995.

(37) (a) Verlet, L. *Phys. Rev.* **1967**, *159*, 98. (b) Swope, W. C.; Andersen, H. C.; Berens, P. H.; Wilson, K. R. *J. Chem. Phys.* **1982**, *76*, 637.

(38) (a) Shaik, S.; Danovich, D.; Fiedler, A.; Schröder, D.; Schwarz, H. *Helv. Chim. Acta* **1995**, *78*, 1393. (b) Shaik, S.; Filatov, M.; Schröder, D.; Schwarz, H. *Chem. Eur. J.* **1998**, *4*, 193.

(39) Taketsugu, T.; Gordon, M. S. *J. Phys. Chem.* **1995**, *99*, 8462.

(40) See for example: Bondybey, V. E. *Annu. Rev. Phys. Chem.* **1984**, *35*, 591.

(41) McQuarrie, D. A. *Statistical Thermodynamics*; University Science Books: Mill Valley, CA, 1973.

(42) Priestley, N. D.; Floss, H. G.; Froland, W. A.; Lipscomb, J. D.; Williams, P. G.; Morimoto, H. *J. Am. Chem. Soc.* **1992**, *114*, 7561.